Ultrasonics 98 (2019) 82–87

Contents lists available at ScienceDirect

Ultrasonics

journal homepage: www.elsevier.com/locate/ultras

Three-dimensional SAFT imaging for anisotropic materials using photoacoustic microscopy

K. Nakahata[a,*], K. Karakawa[a], K. Ogi[a], K. Mizukami[a], K. Ohira[b], M. Maruyama[c], S. Wada[c], T. Namita[d], T. Shiina[d]

[a] Graduate School of Science and Engineering, Ehime University, 3 Bunkyo, Matsuyama, Ehime 790-8577, Japan
[b] Research and Development Center, Japan Probe Co., Ltd., 1-1-14 Nakamura, Yokohama, Kanagawa 232-0033, Japan
[c] Center for Advanced Photonics, RIKEN, 2-1, Hirosawa, Wako, Saitama 351-0198, Japan
[d] Graduate School of Medicine, Kyoto University, 53 Shogoin Kawahara-cho, Sakyo-ku, Kyoto, Kyoto 606-8507, Japan

ARTICLE INFO

Keywords:
Photoacoustic microscopy (PAM)
Synthetic aperture focusing technique (SAFT)
Carbon fiber reinforced plastic (CFRP)
Anisotropy
Subsurface flaw

ABSTRACT

A pulsed laser illuminates a target zone that causes rapid thermoelastic expansion, generating broadband high-frequency ultrasonic wave (photoacoustic wave, PA wave). We developed a PA microscopy (PAM) with a confocal area of laser and ultrasonic wave for applications in nondestructive testing (NDT). The synthetic aperture focusing technique (SAFT) is applied in the PAM for the three-dimensional (3D) imaging of interior flaws. Here, we report proof-of-concept experiments for the NDT of a subsurface flaw in a thin laminar material. Graphical abstract (a) shows a specimen of carbon-fiber-reinforced plastic (CFRP) with an artificial delamination. Here, it should be noted that the group velocity varies directionally due to the strong anisotropy of the CFRP specimen (see Graphical abstract (b)). By considering the group velocity distribution in the SAFT, the shape and location of the subsurface delamination were accurately estimated as shown in Graphical abstract (c). Coating the surface of the CFRP specimen with a light-absorbent material improved the amplitude of the PA wave. This finding showed that the signal-to-noise ratio of the waves scattered from the flaws can be improved.

1. Introduction

Carbon-fiber-reinforced plastic (CFRP) is a composite material of laminated sheets (prepregs) of carbon fibers and epoxy resin. Therefore, CFRPs exhibit a wide variety of composite forms with specific properties [1]. The flaws that occur in-service include matrix micro-cracks, delamination, fiber breakage and fiber-matrix debonding. The characteristics of these flaws are different from those encountered in other homogeneous materials. Various nondestructive testing (NDT) methods have been proposed and developed for assessing internal damages in CFRP laminates [2,3]. Ultrasonic testing (UT) is one of the promising methods for investigating interior flaws because the superior penetrating power of ultrasonic waves with frequencies ranging from hundreds of kHz to several tens of MHz can detect substantial flaws in CFRP [4]. In the pulse-echo configuration of UT, the ultrasonic wave is excited and received with a single transducer. However, the detection of subsurface flaws is sometimes challenging because the trailing signal from the surface interferes with the scattered signal from the flaws [5,6].

Lasers have been used for the NDT of composite materials for the last few decades [7]. The interaction of the material under test with pulsed lasers is known to generate thermoelastic waves (photoacoustic waves) or photomechanical waves (laser-induced stress waves), depending on the intensity of the irradiating laser. These photomechanical waves are generated by the ablation of the material. Although these ablations have a significant effect on the target material, several laser UT methods using photomechanical waves have been reported [8,9]. Photoacoustic (PA) waves are smaller than photomechanical waves and are used for the evaluation of interior flaws in fully-optical systems using an interferometer [10]. In the medical field, PA waves have been actively studied, and photoacoustic microscopy (PAM) [11] has been developed as a tool for PA imaging. In PAM, a laser illuminates the target zone first, then the generated PA wave is detected using an ultrasonic transducer.

In this study, PA is applied to the flaw imaging of CFRP. Here, we develop an original PAM for NDT. The PAM employs a confocal arrangement [12] of optical lenses and ultrasonic transducers to maximize the intensity of the PA wave. The generation of the PA wave depends on the optical and thermal characteristics of the target material. Unlike imaging for human inspection, light cannot penetrate the

* Corresponding author.
E-mail address: nakahata@cee.ehime-u.ac.jp (K. Nakahata).

https://doi.org/10.1016/j.ultras.2019.05.006
Received 22 August 2018; Received in revised form 1 March 2019; Accepted 19 May 2019
Available online 10 June 2019
0041-624X/

deep portion of CFRP. In this study, first the light-absorption coefficient and Grüneisen parameter of the CFRP were investigated. The result shows that a PA wave is mainly generated at the surface of the CFRP. Therefore, we adjusted the PAM so that both optical and ultrasonic waves are focused on the surface of the CFRP. Utilizing the spread of the PA wave from the laser irradiation point, we propose a flaw imaging method based on the synthetic aperture focusing technique (SAFT) [13,14]. Here it is necessary to carefully consider a direction-dependent group velocity [15,16] in the SAFT due to the strong anisotropy of the CFRP. To verify the performance of the proposed method, a subsurface delamination embedded in a CFRP was prepared, and the three-dimensional (3D) shape reconstructions of the delamination was discussed.

2. Photoacousitc (PA) waves in CFRP

2.1. Unidirectional CFRP specimen

In this paper, the Cartesian coordinate $\boldsymbol{x} = (x, y, z)$ is denoted by subscripted variables (x_1, x_2, x_3). The indicial notation is used to represent vectors and tensors, and their mathematical operations. A carbon-epoxy composite plate comprising carbon fibers (Toray Industries, T800S) and epoxy resin (Toray Industries, #2592) was used as a specimen to investigate SAFT imaging. As shown in Fig. 1(a) and (b), the plate has a $[90^{\circ}_{16}]$ lay up using 16 prepreg sheets. That is, the specimen is plastic unidirectionally reinforced with carbon fibers. The composite laminate was cured in an autoclave at a temperature of 130 °C and a pressure of 0.5 MPa. The unidirectional CFRP (UD-CFRP) gives a total thickness of approximately 2 mm. The diameter of the carbon fibers was approximately 6 μm, as shown in Fig. 1(c), with the orientation of the fiber along the x_2 axis. The volume density was about 1600 kg/m^3. An artificial delamination was embedded in the UD-CFRP specimen. To form the delamination, the fluoride resin sheet between the 4th and 5th plies was removed after curing. The size of the delamination was 10 mm × 29 mm.

2.2. Generation of PA waves

The profile of the generated PA signal can be determined by a pulsed laser. For efficient coupling of thermal energy with acoustic waves, the pulse duration must be shorter than the thermal relaxation time. The differences in the light-absorption coefficient μ and the Grüneisen parameter Γ of materials modulate the amplitudes of the PA signal, but the signal profiles are not modulated. The Grüneisen parameter (dimensionless) is expressed as

$$\Gamma = \frac{\alpha K}{C_p \rho} \tag{1}$$

where C_p is the principal heat capacity at constant pressure, α is the volumetric thermal expansion coefficient, K is the bulk modulus, and ρ is the density. The Grüneisen parameter Γ of the CFRP and water [17] are listed in Table 1. The Grüneisen parameter for the CFRP was calculated with the rule of mixtures for unidirectionally reinforced composite materials[18]. The light-absorption coefficient of water is approximately 0.45× 10^{-3} cm^{-1} for laser light at a wavelength of 532 nm [19]. By contrast, CFRP is a bad transparent material for the 532-nm laser light. We estimate the light-absorption coefficient to be approximately 200 cm^{-1} for the 532-nm laser light [10]. The thermoelastic stress in the light absorbent material has an exponential profile in the x_3 axis [20] given by

$$p(x_3) = \Gamma \mu F \exp(-\mu x_3) \tag{2}$$

where F is the fluence of the laser. A schematic image of the stress distribution is shown in Fig. 2. The stress distribution in Eq. (2) acts as a source of the stress waves propagating in both $-x_3$ and $+x_3$ axes. As can be seen in Table 1, the Grüneisen parameter for the CFRP is approximately 2.5 times larger than that of water. The optical absorption coefficients of the CFRP and water are widely different. Considering these parameters, we can assume that the PA wave is generated mainly at the surface of the CFRP specimen. Based on this assumption, we adjusted the microscope so that both optical and acoustical beams are focused on the surface of the CFRP specimen.

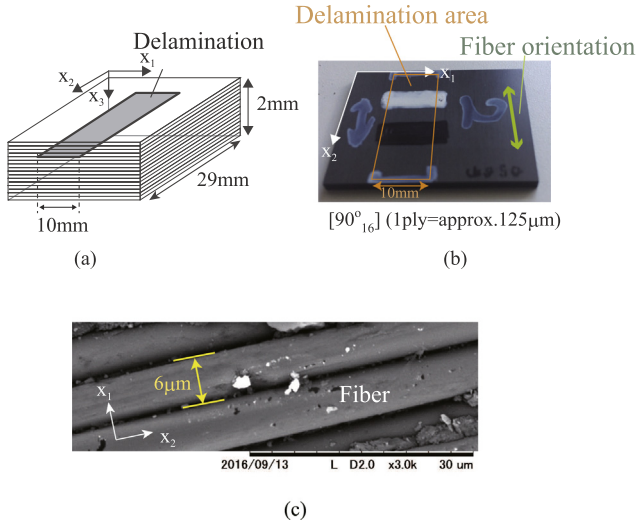

Fig. 1. (a) Unidirectional CFRP specimen with artificial delamination, (b) picture of the specimen, and (c) scanning electron microscope image of the specimen.

2.3. Wave velocity

It is important to consider group velocity when dealing with anisotropic media. The group velocity for a propagation direction $\boldsymbol{n}$ can be obtained using the following equation.

$$g_j^{\alpha} = \frac{1}{\rho v^{\alpha}} c_{ijkl} d_i d_l n_k, \quad (\alpha = \mathrm{P},\ \mathrm{S1},\ \mathrm{S2}) \tag{3}$$

where $\boldsymbol{c}$ is the material stiffness tensor, $\boldsymbol{d}$ is the polarization vector, and v^{α} is the phase velocity of three different types of waves. Einstein's summation convention was applied in Eq. (3). There are waves with mostly longitudinal polarization and two shear waves with mostly transverse polarizations in a general anisotropic material. The longitudinal wave type is referred to as pressure (P) and the other two shear waves are called shear 1, 2 (S1, S2).

For the UD-CFRP, it is appropriate to assume a composite laminate structure as a homogenous body because the wavelength is much greater than the diameter of a carbon fiber. However, the wave velocity and its directional dependence vary due to the fiber orientation and volume fraction. In this study, the two-scale homogenization method [21], based on the asymptotic expansion of field variables, was used to obtain the homogenized elastic constants for the UD-CFRP specimen. The calculated homogenized elastic constants are given as:

$$\begin{Bmatrix} c_{1111} & c_{1122} & c_{1133} & 0 & 0 & 0 \\ c_{1122} & c_{2222} & c_{1122} & 0 & 0 & 0 \\ c_{1133} & c_{1122} & c_{1111} & 0 & 0 & 0 \\ 0 & 0 & 0 & c_{1212} & 0 & 0 \\ 0 & 0 & 0 & 0 & c_{1313} & 0 \\ 0 & 0 & 0 & 0 & 0 & c_{1212} \end{Bmatrix} = \begin{Bmatrix} 15.9 & 6.41 & 9.1 & 0 & 0 & 0 \\ 6.41 & 181 & 6.41 & 0 & 0 & 0 \\ 9.1 & 6.41 & 15.9 & 0 & 0 & 0 \\ 0 & 0 & 0 & 7.64 & 0 & 0 \\ 0 & 0 & 0 & 0 & 3.8 & 0 \\ 0 & 0 & 0 & 0 & 0 & 7.64 \end{Bmatrix} \text{[GPa]}. \tag{4}$$

Table 1
Grüneisen parameters for the CFRP and water [17].

	Specific heat at constant pressure [J/kg/K]	Bulk modulus [GPa]	Coefficient of thermal expansion $\times 10^{-5}$ [1/K]	Density [kg/m^3]	Grüneisen parameter
CFRP	844	8.6	4.1	1545	0.27
Water (25 °C)	4177	2.2	21	997	0.11

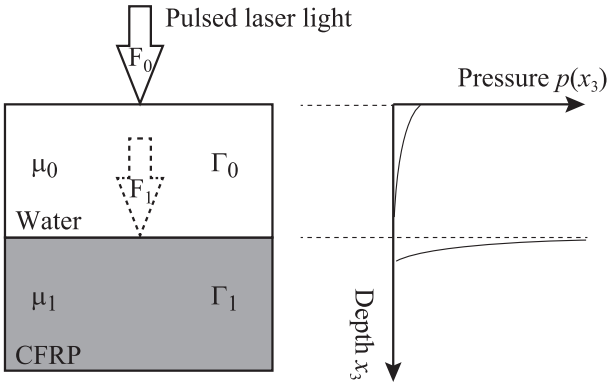

Fig. 2. Generation of thermoelastic stress when a pulsed laser is absorbed in materials.

For a given direction $\boldsymbol{n}$, the phase velocity v^{α} and the corresponding polarization vector $\boldsymbol{d}$ can be obtained by solving an eigenvalue problem based on the Christoffel equation [22]. Using the obtained values v^{α} and $\boldsymbol{d}$, and the given values $\boldsymbol{c}$ and $\boldsymbol{n}$, we can calculate the group velocity for the UD-CFRP specimen The calculated group velocity $\boldsymbol{g} = (g_1, g_2, g_3)$ of the P wave is plotted in Fig. 3. In Fig. 3, the P wave in the x_2 axis propagates at a significantly high velocity, whereas the P wave in the x_1 axis propagates at a lower velocity. This difference is related to the microstructure of CFRP, such that the P wave propagation is faster in the direction of the fiber alignment (x_2) and slower in directions where the wave interacts with the fiber and the matrix (x_1 and x_3). Conversely, the P wave propagates with the same velocity in the x_1–x_3 plane. Accordingly, the specimen has the property of transversely isotropic material.

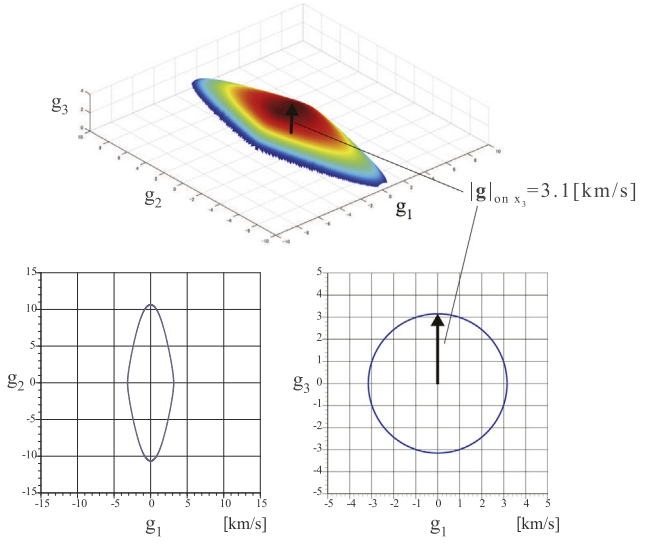

Fig. 3. Group velocity of the P wave in the UD-CFRP specimen.

3. Imaging algorithm using photoacoustic microscopy

3.1. Photoacoustic microscopy (PAM)

An original PAM system for CFRP imaging is illustrated in Fig. 4. This system is based on an acoustic-resolution PAM [12]. The generation of laser light is driven by a compact Q-switched Nd:YAG laser operating at approximately 0.6 mJ pulse energy and 100-Hz pulse repetition rates (Nano L90-100, Litron). The laser emits 4-ns long pulses at a wavelength of 532 nm. The laser emission is controlled by an external trigger signal output from a scanner controller. As shown in Fig. 5, the light at the fiber output end is collimated and reshaped using an axicon lens (83-781, Edmund Optics) to form a ring pattern. The ring-shaped light is then focused onto the target using a reflecting prism (OPL-PAM/532-CL-00, OPTO-LINE). The generated PA waves are detected using an ultrasound transducer (V214-BB-RM, Olympus) located at the center of the prism. In practice, an acoustic lens was attached to the transducer element to focus the ultrasonic beam. The center frequency and the diameter of the transducer are 50 MHz and 6 mm, respectively. As described in the previous section, the foci of the laser excitation and ultrasonic detection are set to the same distance in order to maximize the intensity of the generated PA waves. The measured signal is amplified and digitized using a data acquisition (DAQ) board at a sampling rate of 500 MS/s. A two-dimensional (2D) raster scan is implemented by translating the microscope unit. During the scan, the microscope unit moves in the x_1 and x_2 axes, while the distance between the prism lens and the specimen is kept constant. At each position, the branched optical signal is recorded using a photodetector (DET10A/M, Thorlabs) to correct for any uncertainty in the laser intensity and jitter.

3.2. Synthetic aperture focusing technique (SAFT)

Time-domain SAFT has been applied in ultrasonic NDE because it is capable of improving lateral resolution in the target area[13]. The basic theory of the SAFT for isotropic materials was well summarized by Nikolov [14]. In this section, a 3D SAFT for anisotropic materials is proposed and its concept is shown below. The position vector $\boldsymbol{x} = (x_1, x_2, x_3)$ is defined in the Cartesian coordinates. From previous investigations, the PA wave generates on a CFRP surface. Therefore, we formulate the SAFT under the assumption that the spot size of the laser irradiation is infinitesimal. The position vector $\boldsymbol{o}^n$ indicates the laser irradiation point as shown in Fig. 6. Now, we consider a target voxel of the image reconstruction, which is located at position $\boldsymbol{x}^p$. The time of the PA wave generation is defined as $t = 0$. When the PA wave reaches $\boldsymbol{x}^p$ and be backscattered, the scattered wave is detected after a time t_p (the round-trip interval between the surface and the target voxel).

$$t_p(\boldsymbol{o}^n) = \frac{2}{|\boldsymbol{g}(\boldsymbol{x}^p - \boldsymbol{o}^n)|}\sqrt{(x_i^p - o_i^n)(x_i^p - o_i^n)} \tag{5}$$

where $\boldsymbol{g}(\boldsymbol{x}^p - \boldsymbol{o}^n)$ is the group velocity in the direction from $\boldsymbol{o}^n$ toward $\boldsymbol{x}^p$, which was shown in Eq. (3). Assuming that PA wave is a pulse $\delta(t)$ and the target is a point scatter, the scattered wave shows a scaled and delayed pulse. In this research, the scattered wave is received by ultrasonic transducer at the same position $\boldsymbol{o}^n$ as the laser irradiation point. The signal can be expressed as

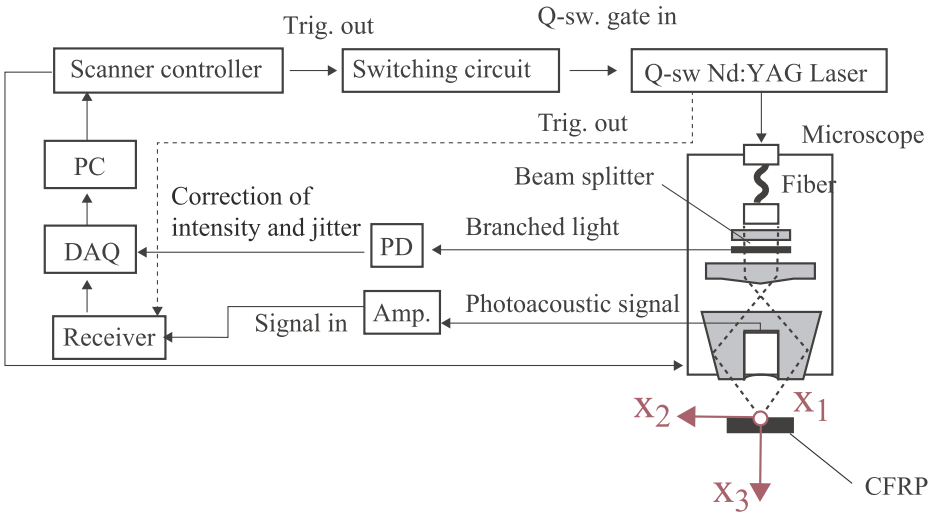

Fig. 4. Flow diagram of the PAM system.

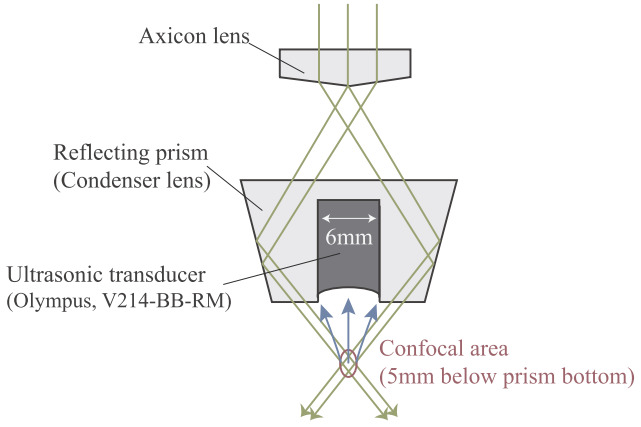

Fig. 5. Detailed view of the microscope.

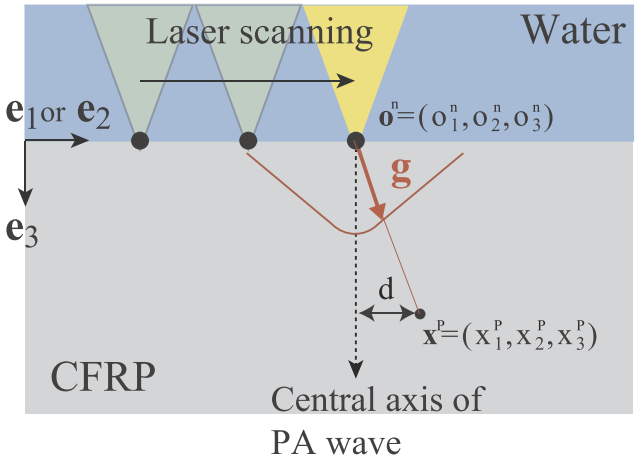

Fig. 6. Wave velocity distribution and intensity of the PA wave in the SAFT.

$$h_p(t, \boldsymbol{o}^n) = c_p \delta(t - t_p) = c_p \delta\left(t - \frac{2}{|\boldsymbol{g}(\boldsymbol{x}^p - \boldsymbol{o}^n)|}\sqrt{(x_i^p - o_i^n)(x_i^p - o_i^n)}\right) \quad (6)$$

where c_p is the backscattering coefficient, The received signal at the transducer position $\boldsymbol{o}^n$ contains scattered waves from various points, and becomes

$$h(t, \boldsymbol{o}^n) = \sum_p^P h_p(t, \boldsymbol{o}^n) \quad (7)$$

where P is the total number of target voxel. Using the received signal h, the reconstructed image H at the target voxel is calculated as a sum over all the receiving points n in this SAFT:

$$H(\boldsymbol{x}^p) = \sum_n^N w(\boldsymbol{o}^n, \boldsymbol{x}^p) h(t_p, \boldsymbol{o}^n) \quad (8)$$

where N is the total number of laser irradiation points. In Eq. (8), w shows the beam intensity factor. Since the spread of the PA wave covers a specific area beneath of the laser irradiation point, we assume the intensity of the PA wave. Here we can express the beam intensity factor as the following Gaussian function

$$w(\boldsymbol{o}^n, \boldsymbol{x}^p) = \exp\left[-\frac{d^2}{(d_0/2)^2}\right] \quad (9)$$

where d_0 is the beam width, and d is the distance between $\boldsymbol{x}^p$ and the beam central axis (see Fig. 6).

4. Results of PA imaging

4.1. Intensity of the PA wave and its frequency properties

Intensities of the generated PA waves were verified using two types of permanent marker inks painted on the surface of the CFRP specimen (as shown in Fig. 7(a)), denoted as points A and C to represent the areas coated with white and black ink, respectively. An imperceptible PA wave is generated at point A, where the white ink is applied, as shown in Fig. 8(a). Conversely, a high-intensity PA wave is detected at point C,

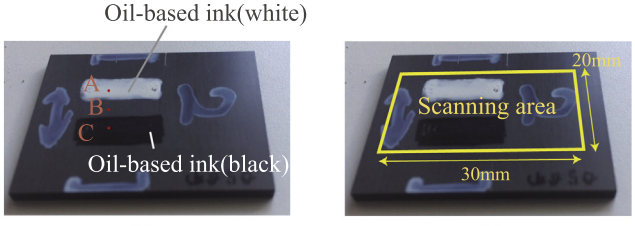

Fig. 7. (a) Photograph of the CFRP specimen on which permanent marker inks were painted. Points A, B and C are in the area of white ink-coated, non-coated, and black ink-coated areas, respectively. (b) Scanning area for the SAFT imaging.

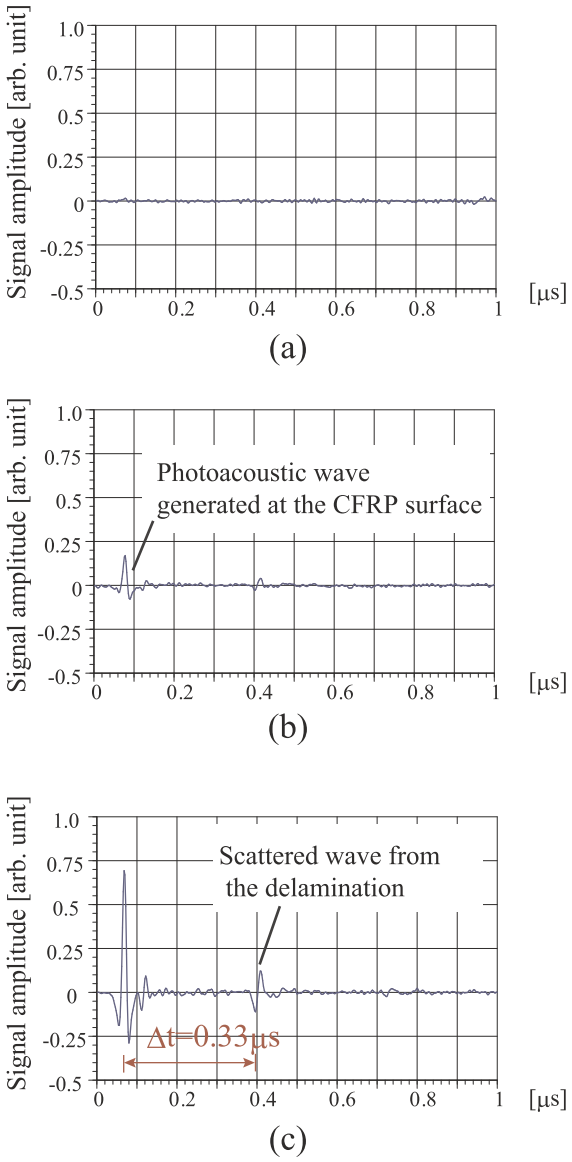

Fig. 8. A-scan images obtained at (a) points A, (b) B, and (c) C.

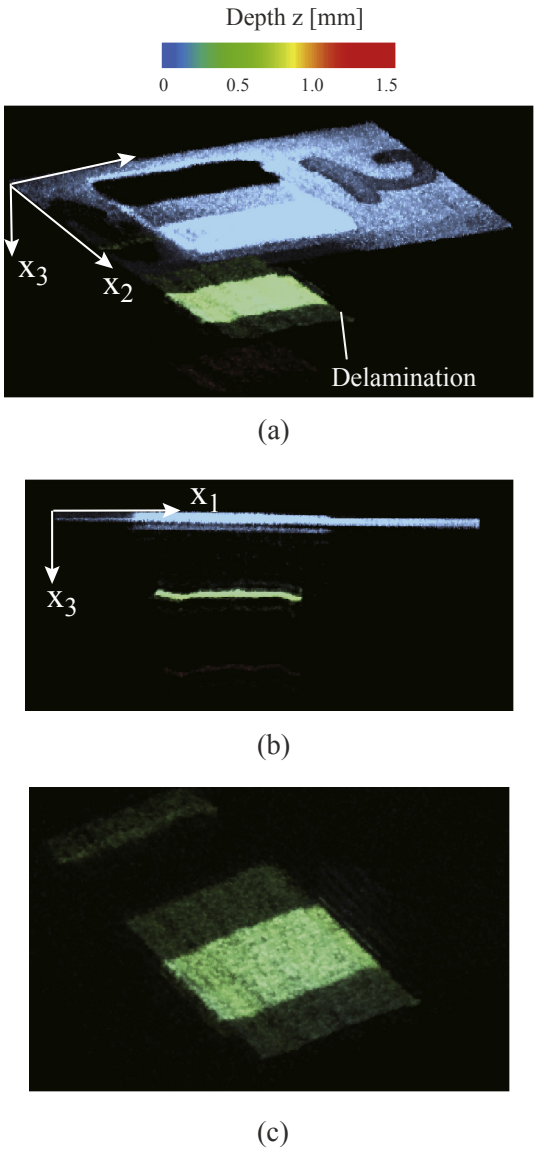

Fig. 9. Results of SAFT imaging for a scanning pitch of 0.05 mm; (a) 3D and (b) cross-sectional images of the CFRP specimen, (c) close-up image of the delamination.

coated with permanent black ink, as shown in Fig. 8(c). At point B in the non-coated area shown in Fig. 8(b), we can see a small PA wave. The difference in the amplitude results from the optical and thermal characteristics of the black and white inks.

Next, we checked the validity of the group velocity, as shown in Fig. 3. The delamination is located between the fourth and fifth plies of the specimen. The depth of the delamination is approximately 0.5 mm. Since the group velocity in the x_3 axis is 3.1 km/s, the round-trip time of the PA wave from the delamination is estimated as 0.33 μs ($= 2 \times 0.5$ [mm]/3.1 [km/s]). The estimated round-trip time showed good agreement with the time interval in Fig. 8(c).

4.2. SAFT Imaging of subsurface delamination in the CFRP

This section demonstrates 3D SAFT imaging in the CFRP specimen. As shown in Fig. 7(b), the raster scan is performed in an area 30 mm × 20 mm. In 2D raster scanning, the microscope unit is translated at 0.05 mm pitch with a constant moving speed. Since the laser is irradiated with 100-Hz pulse repetition rates, the moving speed of microscope is 5 mm/s (thetotal scanning time is approximately 58 min). The minimum wavelength of the PA wave at a frequency 50 MHz is about 0.06 mm, thus the scanning pitch is approximately the same as the wavelength. In each point, only one shot of laser is performed, therefore signal average processing is not introduced. The 3D images in the CFRP specimen, as shown in Fig. 9 were obtained using the software, KURUMI [23]. The spatial resolution along the x_1 and x_2 axes are both 0.05 mm, while the step along the x_3 axis is 0.005 mm. The beam width d_0 in the SAFT is set to 0.2 mm. The reconstructed value $H(\boldsymbol{x})$ over a threshold is plotted in Fig. 9. In this case, $H(\boldsymbol{x})$ was normalized by the maximum value in the reconstruction area. Here we selected 0.4 as the threshold value. The color and brightness indicate the depth of the scatterer and the intensity of the scattered wave, respectively. In Fig. 9(a), the location and shape of the delamination and bottom surface were reconstructed with high accuracy. The cross-sectional view of the delamination is shown in Fig. 9(b). It was observed that the depth of the delamination was correctly estimated. A close-up image of the delamination is illustrated in Fig. 9(c). Horizontal stripes corresponding to the orientation of the carbon fibers can be observed along the x_2 axis in Fig. 9(c). Fig. 10 shows 3D images in the CFRP specimen with a scanning pitch of 0.2 mm (the moving speed of microscope is 20 mm/s, and the total scanning time is approximately 6 min.). The other conditions

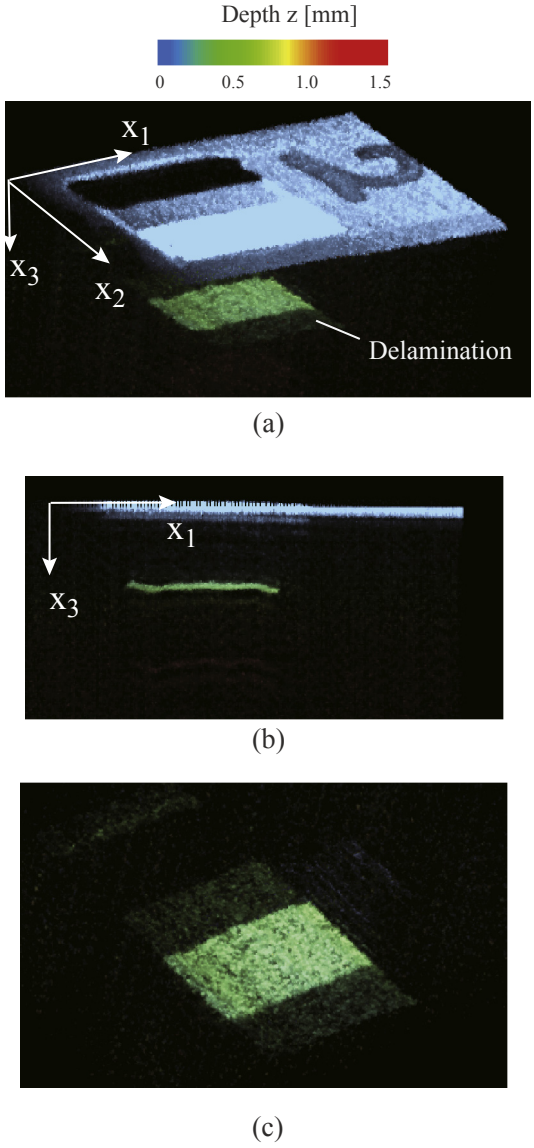

Fig. 10. Results of SAFT imaging for a scanning pitch of 0.2 mm; (a) 3D and (b) cross-sectional images of the CFRP specimen, (c) close-up image of the delamination.

in the SAFT are the same, as in Fig. 9. Although the scanning pitch in Fig. 10 is four times larger than that in Fig. 9, the location and shape of the delamination can be reconstructed clearly.

From these results, it was observed that the SAFT images obtained using PAM show the accurate location of the delamination. Our method offers vertical high-resolution images because of the wide frequency band of the PA waves generated by the pulsed-laser irradiation. It is capable of improving lateral resolution in the focal zone using the SAFT algorithm. Furthermore, the shape of the delamination under the black permanent ink was clearly reconstructed. When a strong optical absorber, such as black ink, lies on the specimen, the amplitude of the wave scattered from the delamination increase in intensity relative to the amplitude of the signal reflected from the non-coated CFRP surface. A light absorbent coating on the specimen surface improves the signal-to-noise (S/N) ratio of the waves scattered from the flaw.

5. Summary

We proposed a 3D SAFT imaging method for nondestructive testing using PAM. In the PAM, a confocal area of light and ultrasonic wave was designed, and a 532-nm wavelength laser, with 4-ns pulse duration, was irradiated at the top surface of the specimen. PA waves in the ultrasonic range were received using an immersion transducer on the same side. In the SAFT, a three-directionally varying group velocity in the unidirectional CFRP specimen was considered. The SAFT imaging using PAM showed the exact location and shape of delaminations. Our method offers vertical high-resolution images because of the wide frequency band of the acoustic wave generated by the pulsed-laser irradiation. It is capable of keeping the lateral resolution in the focal zone using a SAFT algorithm in the case of rough scanning pitch. It should be noted that the intensity of the generated ultrasonic waves is affected by the optical properties of the target material. By coating a light absorbent material on the surface, a strong ultrasonic wave can be generated from the surface of the CFRP into the interior of the sample in order to improve the S/N ratio of the signal scattered from the flaw. Our future work will include a determination of appropriate parameters while performing the SAFT imaging. We will also apply an air-coupled transducer as detector for non-contact NDT.

Acknowledgments

This study was funded by the ImPACT Program (Project manager: Takayuki Yagi) of the Council for Science, Technology and Innovation (Cabinet Office, Government of Japan).

References

[1] B. Fiedler, C. Jong, T. Hobbiebrunken, M. Hojo, K. Schulte, Micro/ macro-mechanical approach of first ply failure in CFRP, J. Mater. Sci. 41 (2006) 6760–6767.
[2] L. Cheng, G.-Y. Tian, Comparison of nondestructive testing methods on detection of delaminations in composites, J. Sens. 1 (2012) 408437.
[3] S. Gholizadeh, A review of non-destructive testing methods of composite materials, in: Procedia Structural Integrity (Proceedings of XV Portuguese Conference on Fracture 2016), vol. 1, 2016, pp. 50–57.
[4] R. Smith, Composite defects and their detection, Mater. Sci. Eng. 3 (2009) 103–143.
[5] X. Gros, K. Ogi, K. Takahashi, Eddy current, ultrasonic C-scan and scanning acoustic microscopy testing of delaminated quasi-isotropic CFRP materials: a case study, J. Reinf. Plast. Comp. 17 (5) (1998) 389–405.
[6] Q. Shen, M. Omar, S. Dongri, Ultrasonic NDE techniques for impact damage inspection on CFRP laminates, J. Mater. Sci. Res. 1 (1) (2012) 2–16.
[7] C. Scruby, L. Drain, Laser Ultrasonics Techniques and Applications, CRC Press, New York, USA, 1990.
[8] V. Kozhushko, P. Hess, Laser-induced focused ultrasound for nondestructive testing and evaluation, J. Appl. Phys. 103 (2008) 124902.
[9] M. Kalms, O. Focke, C. Kopylow, Applications of laser ultrasound NDT method on composite structures in aerospace industry, in: Proceedings of 9th International Symposium on Laser Metrology, Vol. 7155, 2008, p. 71550E.
[10] I. Pelivanov, T. Buma, J. Xia, C. Wei, M. Donnell, NDT of fiber-reinforced composites with a new fiber-optic pump-probe laser-ultrasound system, Photoacoustics 2 (2) (2014) 63–74.
[11] L. Wang, S. Hu, Photoacoustic tomography: in vivo imaging from organelles to organs, Science 335 (2012) 1458–1462.
[12] H.F. Zhang, K. Maslov, G. Stoica, L.V. Wang, Functional photoacoustic microscopy for high-resolution and noninvasive in vivo imaging, Nat. Biotechnol. 24 (7) (2006) 848–851.
[13] J. Seydel, Ultrasonic Synthetic Aperture Focusing Techniques in NDT vol. 6, Academic Press, 1982, pp. 1–47.
[14] S.I. Nikolov, Synthetic aperture tissue and flow ultrasound imaging, Ph.D. thesis, Technical University of Denmark (Aug. 2002).
[15] M. Spies, W. Jager, Synthetic aperture focusing for defect reconstruction in anisotropic media, Ultrasonics 41 (2003) 125–131.
[16] R.-C. Shih, Y.-F. Chang, C.-H. Chang, P.-Y. Tseng, Ultrasonic synthetic aperture focusing using the root-mean-square velocity, J. Nondestruct. Eval. 33 (2014) 12–22.
[17] National institute of standards and technology. < http://webbook.nist.gov/ > .
[18] R. Christensen, Mechanics of Composite Materials, Dover Publications, New York, USA, 2005.
[19] R.M. Pope, E.S. Fry, Absorption spectrum (380–700 nm) of pure water. II. Integrating cavity measurements, Appl. Opt. 36 (33) (1997) 8710–8723.
[20] G. Paltauf, H. Schmidt-Kloiber, Model study to investigate the contribution of spallation to pulsed laser ablation of tissue, Lasers Surg. Med. 16 (1995) 277–287.
[21] J.M. Guedes, N. Kikuchi, Preprocessing and postprocessing for materials based on the homogenization method with adaptive finite elements methods, Comput. Methods Appl. Mech. Eng. 83 (1990) 143–198.
[22] B.A. Auld, Acoustic Fields and Waves in Solids vol. 1, Krieger Publishing Company, Florida, USA, 1990.
[23] KURUMI (Kyoto University Rapid and Universal MIP Imager). < https://www.kuhp.kyoto-u.ac.jp/~diag_rad/intro/tech/kurumi.html#KURUMI_EN > .